Supporting Information to

Charging of poly(methyl methacrylate) (PMMA) colloids in cyclohexyl bromide: locking, size dependence and particle mixtures

M. N. van der Linden, J. C. P. Stiefelhagen, G. Heessels-Gürboğa,
J. E. S. van der Hoeven, N. A. Elbers, M. Dijkstra and A. van Blaaderen

1 Interaction potential

The pair interaction in a system of charged colloidal particles is commonly described by a hard-core repulsive Yukawa (screened Coulomb) potential [1, 2, 3, 4]:

$$\beta u_{ij}(r) = \begin{cases} \beta\epsilon_{ij} \dfrac{\exp\left[-\kappa(r-\sigma_{ij})\right]}{r/\sigma_{ij}} & r \geq \sigma_{ij} \\ \\ \infty & r < \sigma_{ij} \end{cases} , \tag{1}$$

with $\sigma_{ij} = (\sigma_i + \sigma_j)/2$ and the contact value of the potential between two colloids i and j:

$$\beta\epsilon_{ij} = \frac{Z_i Z_j}{(1+\kappa\sigma_i/2)(1+\kappa\sigma_j/2)} \frac{\lambda_\mathrm{B}}{\sigma_{ij}} , \tag{2}$$

where r is the centre-to-centre distance between particles i and j, Z_i (Z_j) and σ_i (σ_j) are the charge number and diameter of colloid i (j), $\beta = 1/(k_\mathrm{B}T)$, with k_B the Boltzmann constant, and T the absolute temperature. The Bjerrum length is given by

$$\lambda_\mathrm{B} = \frac{e^2}{4\pi\epsilon_\mathrm{r}\epsilon_0 k_\mathrm{B}T} , \tag{3}$$

with e the elementary charge, ϵ_r the relative dielectric constant of the solvent and ϵ_0 the dielectric permittivity of vacuum. The Bjerrum length represents the distance at which the electrostatic interaction energy between two monovalent ions is equal to the thermal energy $k_\mathrm{B}T$. The inverse Debye screening length is given by

$$\kappa = \sqrt{8\pi\lambda_\mathrm{B} c_\mathrm{s}} , \tag{4}$$

with c_s the concentration of the monovalent salt. The Debye screening length κ^{-1} indicates the thickness of the electrical double layer surrounding a colloidal particle and is a measure for the interaction range between two colloids. When the refractive index of the solvent closely matches that of the

particles, as is the case in our experimental system, the Van der Waals interactions are much smaller than $k_{\mathrm{B}}T$ and can be neglected.

The electrostatic surface potential $\psi_{0,\,i}$ for an isolated particle i can be approximated at low $\psi_{0,\,i}$ by [5]

$$\beta e\psi_{0,\,i} = \frac{Z_i}{1+\kappa\sigma_i/2}\,\frac{2\lambda_{\mathrm{B}}}{\sigma_i}\,. \tag{5}$$

2 Ion concentration

If we consider the dissociation of a monovalent salt:

$$\mathrm{AB} \rightleftarrows \mathrm{A^+} + \mathrm{B^-}\,, \tag{6}$$

then the law of mass action applied to this equilibrium yields the following expression for the dissociation constant:

$$K_{\mathrm{D}} \approx \frac{[\mathrm{A^+}][\mathrm{B^-}]}{[\mathrm{AB}]} = \frac{(\alpha c_0)^2}{(1-\alpha)c_0}\,, \tag{7}$$

with K_{D} the dissociation constant, α the degree of dissociation, $[\mathrm{A^+}]$ and $[\mathrm{B^-}]$ the concentrations of free ions ($\mathrm{A^+}$ and $\mathrm{B^-}$), [AB] the concentration of undissociated ion pairs (AB) and c_0 the total concentration of electrolyte ($c_0 = [\mathrm{A^+}] + [\mathrm{AB}]$). For simplicity we took the ionic activity coefficients to be close to 1, which is a reasonable approximation for low concentrations of free ions. The dissociation constant may be approximated by [6, 7]

$$K_{\mathrm{D}} = \frac{3}{4\pi a^3}\,\exp\left(-\frac{\lambda_{\mathrm{B}}}{a}\right), \tag{8}$$

with a the centre-to-centre distance of the dissociating ion pair and λ_{B} the Bjerrum length (Eq. 3). For small K_{D} ($\alpha \ll 1$), combining Eqs. 7 and 8 yields for the concentration (number density) of free ions

$$[\mathrm{A^+}] + [\mathrm{B^-}] = 2\alpha c_0 \approx \sqrt{\frac{3c_0}{\pi a^3}}\,\exp\left(-\frac{\lambda_{\mathrm{B}}}{2a}\right), \tag{9}$$

where we used $[\mathrm{A^+}] = [\mathrm{B^-}] = \alpha c_0$ and $[\mathrm{AB}] = (1-\alpha)c_0 \approx c_0$. The derivation of Eq. 8 for the dissociation constant was given by Fuoss [6] and was used later by Van der Hoeven and Lyklema [7]. Roberts et al. [8] used an expression similar to Eq. 9 for the concentration of free ions; we note, however, that the prefactor in Ref. [8] differs by a factor $\sqrt{8}$ from the prefactor in Eq. 9, because the ionic radius instead of the ion pair centre-to-centre distance was used.

3 Debye screening length

The conductivity of CHB after the cleaning steps was on the order of 10 pS cm^{-1}. From this, we obtained an estimate of the Debye screening length, in the following way (after Ref. [9] and chapter 2 of Ref. [10]). We assumed that the ions contributing to the conductivity of the solvent were $\mathrm{H^+}$ and $\mathrm{Br^-}$ and that their concentrations were equal ($c_{\mathrm{H^+}} = c_{\mathrm{Br^-}} = c_{\mathrm{s}}$). Furthermore, we assumed independent migration of ions, which should be a reasonable assumption in our dilute solutions. The

Table 1: Viscosities η and limiting molar conductance Λ^0 of HBr in CHB and ethanol (reference solvent). The viscosity of ethanol and Λ^0 in ethanol are literature values from Ref. [12] for $T = 298$ K (see also Refs. [10, 9]); the viscosity of CHB is from Ref. [10] and was measured at $T = 293$ K; Λ^0 in CHB was calculated from Eq. 11.

Solvent	η / (mPa s)	Λ^0 / (cm^2 S mol^{-1})
CHB	2.269	42.3
Ethanol	1.08	88.9

conductivity D (S m^{-1}) is then related to the concentration of free ions through:

$$D = c_\mathrm{s}\ \Lambda^0, \tag{10}$$

where c_s is the concentration (mol m^{-3}) of fully dissociated electrolyte (HBr) (note that the concentration of free ions is $2c_\mathrm{s}$) and Λ^0 is the limiting molar conductance (m^2 S mol^{-1}) of the electrolyte in a particular solvent (CHB), i.e. the molar conductance at infinite dilution (as indicated by the superscript '0'). We used Walden's rule to obtain a (rough) estimate [11] for Λ^0 of HBr in CHB, as we do not know of available literature values. Walden's rule states that the product of the viscosity η_i of a solvent i and the limiting molar conductance Λ_i^0 of an electrolyte in that solvent is the same for different solvents:

$$\Lambda_1^0\ \eta_1 = \Lambda_2^0\ \eta_2, \tag{11}$$

where Λ_1^0 is the (unknown) limiting molar conductance in solvent 1, Λ_2^0 the (known) limiting molar conductance in reference solvent 2, and η_1 and η_2 are the viscosities of the respective solvents. We take ethanol as reference solvent 2, for which the limiting molar conductance of HBr (H^+ and Br^-) is known from literature. Table 1 summarizes the literature values for the viscosities of ethanol and CHB, and the limiting molar conductance of HBr in ethanol, as well as the limiting molar conductance of HBr in CHB, calculated from Eq. 11.

Using the relation between conductivity and ionic strength from Eq. 10 and the value for Λ^0 of HBr in CHB from Table 1, we calculated that a conductivity $D = 10$ pS cm^{-1} corresponds to an ionic strength $c_\mathrm{s} = 2.4 \times 10^{-10}$ mol L^{-1}. This results in a Debye screening length $\kappa^{-1} = 6$ µm (Eq. 4).

4 Incorporation of RITC fluorescent dye

A reviewer brought to our attention that a reaction of isothiocyanates with amines (as performed in Ref. [13] to synthesize the RITC monomer) might be disturbed by side reactions in an (absolute) ethanol solution (see Ref. [14]). The use of ethanol as a solvent for this coupling reaction is however well established in the field of silica modification, as in this field reactions of amines containing silane coupling agents, such as aminopropyltriethoxysilane, with compounds containing isothiocyanate groups are frequently carried out in ethanol as solvent (see e.g. Refs. [15, 16]). Moreover, it was established by our group that performing the coupling of RITC to an amine containing silane coupling agent in ethanol led to incorporation of the dye in silica particles, while no incorporation was achieved without this reaction [16]. In addition, the amount of incorporated isothiocyanate dye that reacted with the silane coupling agent aminopropyltriethoxysilane in a pure form (without ethanol as solvent) as compared to the amount when ethanol was used as solvent, was similar in magnitude [16, 17].

5 Mobility profiles

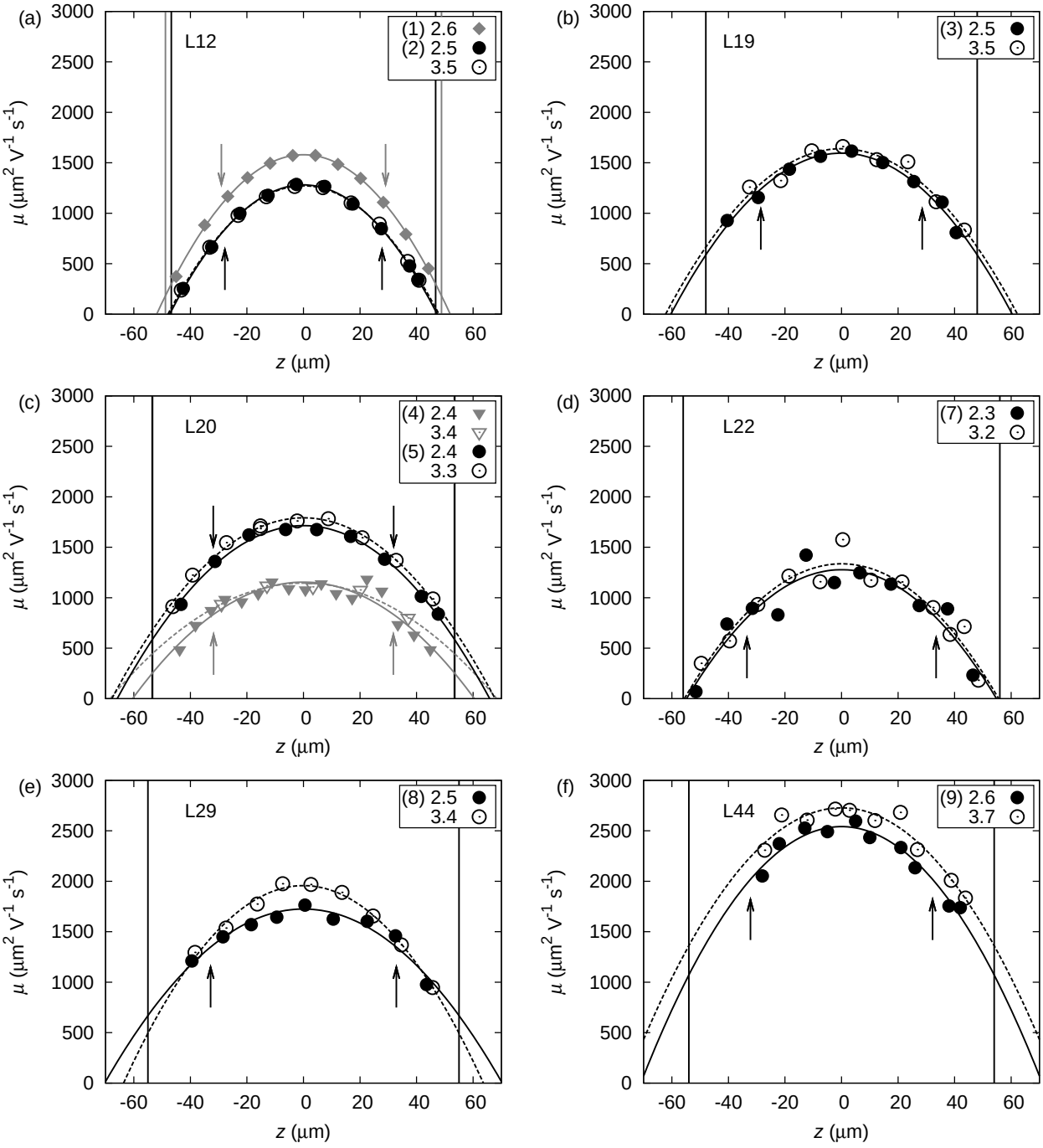

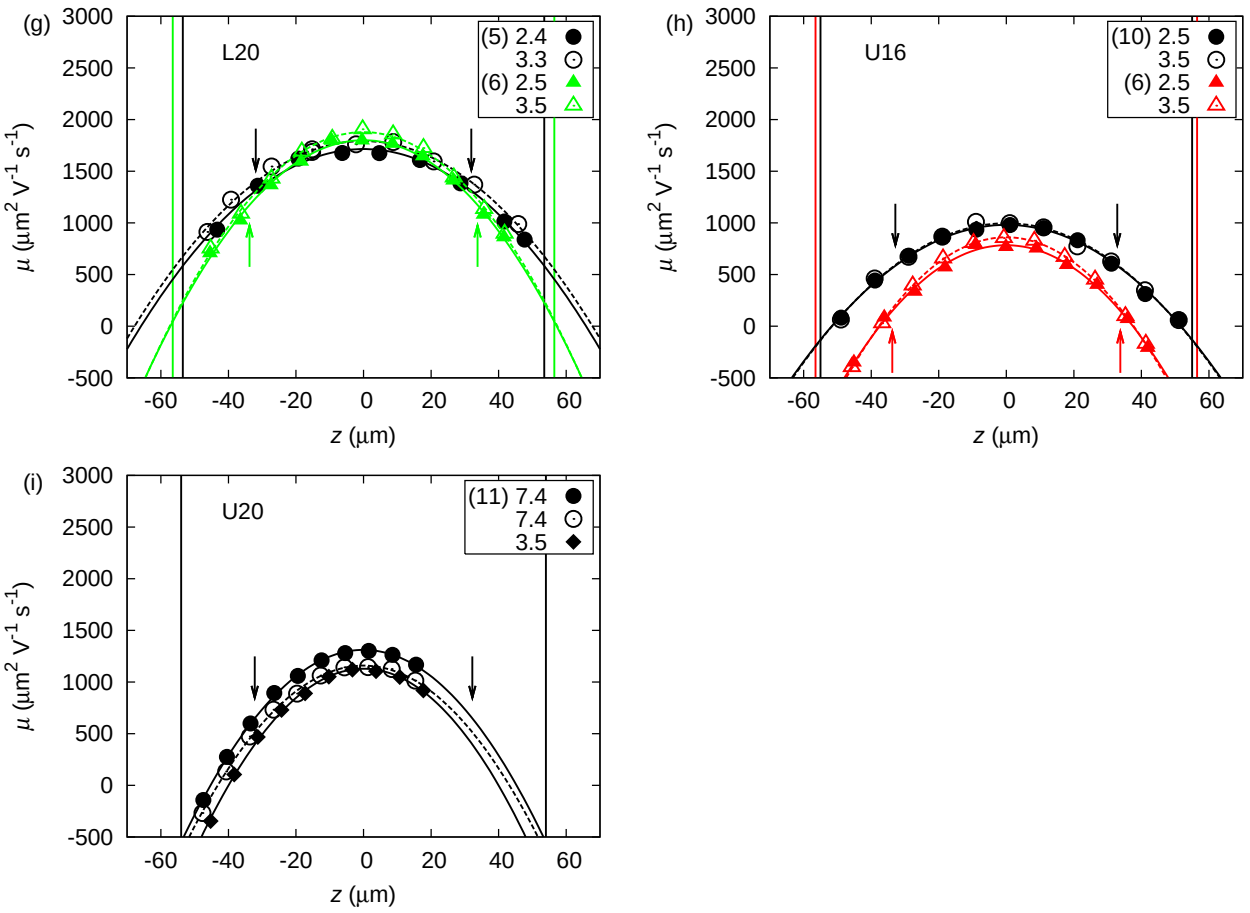

Figure 1: ((a)–(f) on previous page) Mobility profiles for locked and unlocked PHSA-*g*-PMMA-stabilized PMMA particles in CHB, corresponding to the samples reported in Table 1 in the main article: (a) L12, samples 1 and 2; (b) L19, sample 3; (c) L20, samples 4 and 5 (one-component); (d) L22, sample 7; (e) L29, sample 8; (f) L44, sample 9; (g) L20, samples 5 (one-component) and 6 (mixture with U16); (h) U16, samples 10 (one-component) and 6 (mixture with L20); (i) U20, sample 11. Each panel corresponds to one type of particle, as labeled. Panels (g) and (h) show the same data as Figs. 2a and b in the main article. The legend gives the sample number in brackets followed by the field strength E in V mm^{-1}. Each legend entry corresponds to one mobility profile. The vertical lines in each panel indicate the positions of the walls, the arrows indicate the two stationary levels (where the electro-osmotic flow is zero; $z = z_{\mathrm{stat}}$; Eq. 3 in the main article). For all samples except sample 4 the data and fits have been corrected for the contribution of gravity to the apparent mobility of the particles (see Section 2.3 in the main article). For further experimental details see Table 1 in the main article.

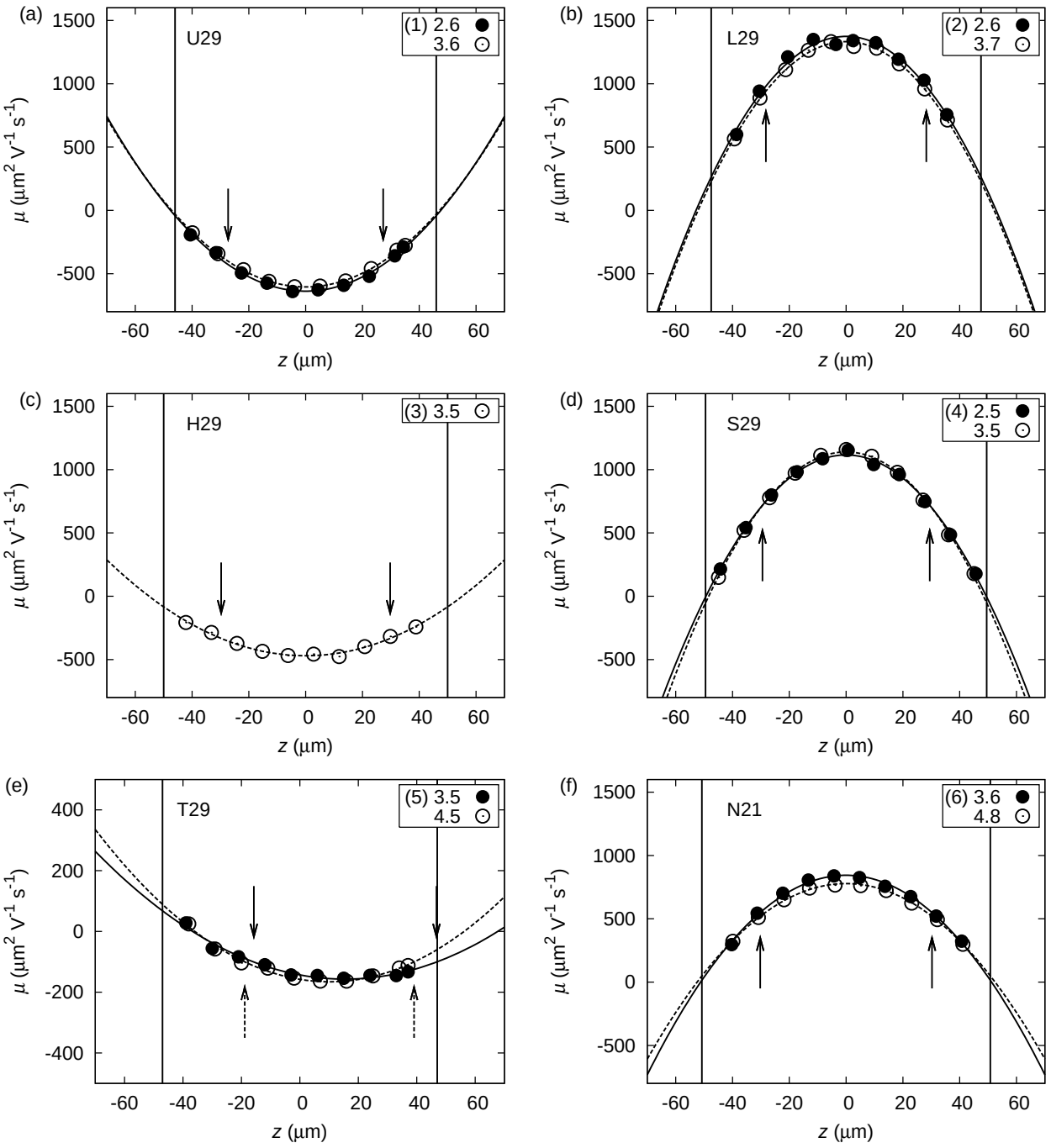

Figure 2: Mobility profiles for PHSA-*g*-PMMA-stabilized PMMA particles in a solvent mixture of CHB and 20 weight-% *cis*-decalin, corresponding to the particle batches reported in Table 2 in the main article: (a) U29, batch 1; (b) L29, batch 2; (c) H29, batch 3; (d) S29, batch 4; (e) T29, batch 5; (f) N21, batch 6. Each panel corresponds to one type of particle, as labeled. The legend gives the batch number in brackets followed by the field strength E in V mm^{-1}. Each legend entry corresponds to one mobility profile. The vertical lines in each panel indicate the positions of the walls, the arrows indicate the two stationary levels (where the electro-osmotic flow is zero; $z = z_{\mathrm{stat}}$; Eq. 3 in the main article). The data and fits have been corrected for the contribution of gravity to the apparent mobility of the particles (see Section 2.3 in the main article). For further experimental details see Table 2 in the main article.

6 Reactions

Fig. 3 shows the locking reaction (left), by which the stabilizer becomes chemically coupled to PMMA, and the esterification reaction of 2-(dimethylamino)ethanol (DMAE) with methacrylic acid (MAA) forming 2-(dimethylamino)ethyl methacrylate (DMAE-MA) (right).

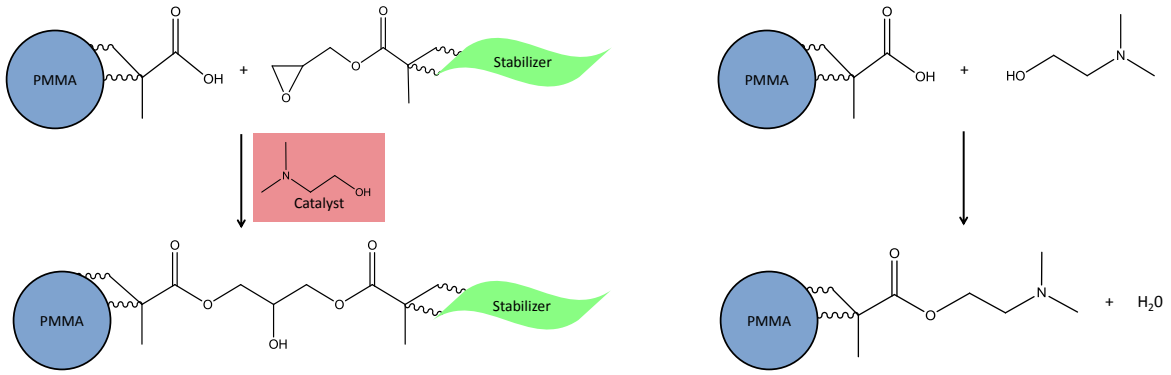

Figure 3: (Left) Locking reaction and (right) esterification reaction.

7 IR and ESI-MS analysis

To test whether the esterification reaction between methacrylic acid (MAA) and 2-(dimethylamino)ethanol (DMAE) could take place in dodecane, we performed a test reaction between MAA and DMAE (molar ratio 1:1) under the same conditions as for the locking procedure. We analyzed the resulting mixture with solution infrared (IR) spectroscopy (Perkin-Elmer Spectrum One FT-IR spectrometer) using pentadecane as a solvent and with electron spray ionization-mass (ESI-MS) spectrometry (Waters LCT Premier XE KE317 Micromass Technologies spectrometer) using dichloromethane acidified with formic acid. The IR spectrum (Fig. 4) showed that an ester was formed (peaks at 1743 cm^{-1} (C=O stretch) and 1294 cm^{-1} (C-O stretch)). The peak at 1700 cm^{-1} corresponds to the C=O stretch of a carboxylic acid group, probably from unreacted MAA. The ESI-MS spectrum showed a peak at an m/z value of 158.12, corresponding to protonated 2-(dimethylamino)ethyl methacrylate. These results show that the ester 2-(dimethylamino)ethyl methacrylate can indeed be formed in dodecane under the conditions of the locking procedure.

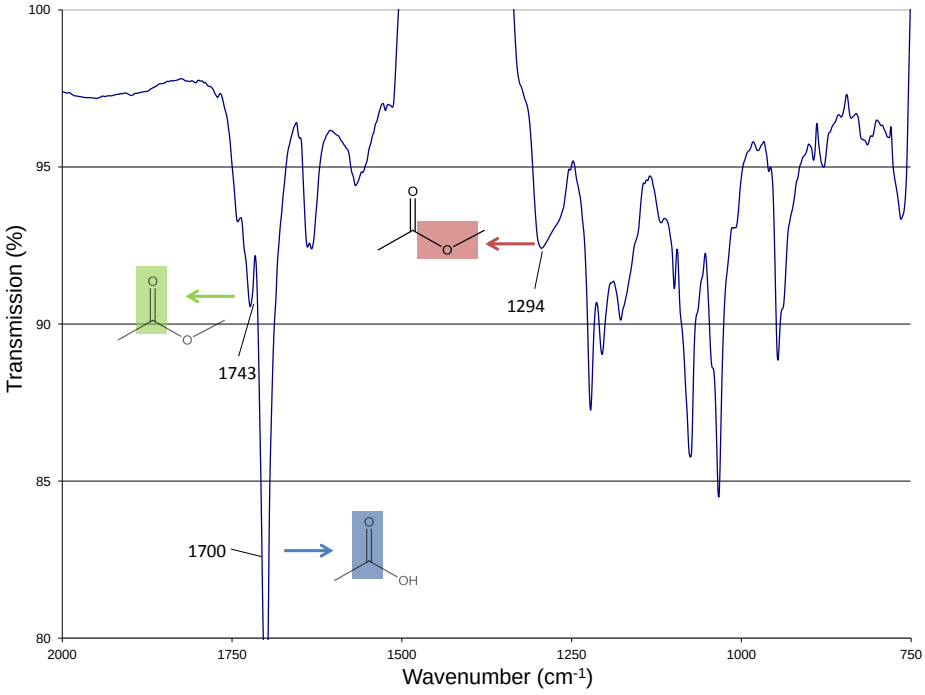

Figure 4: IR spectrum for the resulting reaction mixture after the reaction between methacrylic acid and 2-(dimethylamino)ethanol. The spectrum for the solvent dodecane has been substracted.

8 Experimental details for electrophoresis measurements

The experimental procedure and analysis for the electrophoresis measurements in Table 2 in the main article were similar to those described in Section 2 of the main article.

We note that the electrophoresis measurements in Table 2 in the main article were performed in a mixture of CHB and 20 weight-% *cis*-decalin. This was necessary, as during the sedimentation of some of these particles swirls developed, which destroyed the parabolic flow profiles, making it impossible to determine the particle mobility. The density of CHB/*cis*-decalin is closer to that of PMMA than

Table 2: Experimental details and results for the electrophoresis measurements on PHSA-*g*-PMMA-stabilized PMMA particles in a mixture of CHB and 20 weight-% *cis*-decalin. Details on the preparation method for each batch of particles can be found in Table 2 in the main article. For each batch we report the name of the particle, the mean diameter σ and polydispersity s as determined by static light scattering (SLS; batches 1–5) or scanning electron microscopy (SEM; batch 6), the type of fluorescent dye used to label the particle, the field strengths E at which the measurements were performed, the volume fraction η, the state of the suspension during the measurements (X = crystalline, F = fluid), the mean particle mobility μ_E as determined by electrophoresis, the dimensionless surface potential $\beta e\psi_0$ ($T = 298$ K), and the number of charges on the particle Z, assuming a Debye screening length κ^{-1} of 6 µm. The volume fraction for batches 1–5 was determined from a 3D data set; the volume fraction for batch 6 was estimated from the amounts of PMMA and CHB used for suspension preparation and the measured volume fraction for the other batches, as a 3D data set was not available for batch 6. Batch 5 was inhomogeneous; see text for details. The mobility profiles for all samples can be found in Fig. 2.

Batch no.	Particle	$\frac{\sigma}{\mu\mathrm{m}}$	s (%)	Dye	$\frac{E}{\mathrm{V\,mm^{-1}}}$	η	State	$\frac{\mu_\mathrm{E}}{10^2\,\mu\mathrm{m^2\,V^{-1}\,s^{-1}}}$	$\beta e\psi_0$	Z
1	U29	2.87	2.4	NDB	2.6, 3.6	0.015	F	-4.1 ± 0.1	-2.12 ± 0.06	-280 ± 9
2	L29	2.87	2.4	NDB	2.6, 3.7	0.012	X	$+9.6 \pm 0.2$	$+4.04 \pm 0.07$	$+688 \pm 18$
3	H29	2.87	2.4	NDB	3.5	0.015	F	-3.3	-1.76	-223
4	S29	2.87	2.4	NDB	2.5, 3.5	0.018	F	$+7.18 \pm 0.01$	$+3.59 \pm 0.00$	$+536 \pm 0$
5	T29	2.87	2.4	NDB	3.5, 4.5	0.008	F	-1.00 ± 0.00	-0.40 ± 0.00	-59 ± 0
6	N21	2.09	3.0	RITC	3.6, 4.8	0.015	F	$+5.3 \pm 0.1$	$+3.23 \pm 0.06$	$+266 \pm 8$

the density of pure CHB, which slowed down the sedimentation of the particles sufficiently to prevent the swirls from developing. We expect the surface potential and charge of the particles suspended in CHB/*cis*-decalin to be different from those of the same particles suspended in pure CHB. However, we believe that the effect of the different synthesis and post-synthesis conditions on the charge of the particles will be apparent in both of these solvents. This seems justified, as we found comparable results for particle L29 in CHB (Table 1, sample 8) and CHB/*cis*-decalin (Table 2, batch 2).

As can be seen from Fig. 2e, the maximum of the mobility profiles for particle T29 (batch 5) did not coincide with the middle of the capillary. This was due to the adsorption of particles on one wall of the capillary, when it was kept in a horizontal position during the UV-curing of the glue. During the measurement the particles desorbed from the capillary wall, creating a gradient in volume fraction across the 0.10-mm depth of the capillary. We estimated the positions of the stationary planes in this sample (indicated by arrows in Fig. 2e) by assuming that in the 2D plane of measurement the net fluid velocity was zero (which introduces a small error as it neglects the finite width of the capillary) and by assuming a particle mobility independent of the volume fraction. To calculate the surface potential and charge from the mobility we assumed the volume fraction to be equal to the overall volume fraction. Since the parabolas in Fig. 2e are very shallow, the error in the estimated positions of the stationary planes will be small and we believe it does not affect our conclusions.

9 Locking test

We performed a test to verify the locking for batches L22 and L29 from Table 1 in the main article, which are both locked. The procedure relies on the fact that PMMA dissolves in toluene, but is fully collapsed in pure alkanes. For particles L22 and L29, as well as for the same particles in the unlocked state, we prepared suspensions with $\eta = 0.02$ in toluene. Thirty minutes after preparation, we added

twice the suspension volume of heptane and mixed. After the treatment with toluene and heptane, we used confocal microscopy to look at the particles. We found a clear difference between the locked and unlocked particles: the unlocked particles had deformed and lost their spherical shape, while the locked particles had kept their spherical shape. We conclude from this that for the locked particles the stabilizer was covalently bonded to the PMMA chains of the particle, i.e. that the locking procedure worked.

10 Unlabeled PMMA

To exclude a significant influence from the dye on the particle charge, we prepared a suspension of unlocked particles (diameter = 2.31 µm) consisting of a thick unlabeled PMMA shell and a small fluorescently labeled silica core (diameter = 353 nm; $< 1\%$ of the total mass of the particle) in purified CHB. The RITC dye cannot leak out of the silica core, as it is incorporated covalently in a silica core, which in turn is incorporated in a shell consisting of silica without dye.

We investigated the phase behavior for these PMMA particles at a volume fraction of 0.02. We found that the particles sedimented (upwards, since their density was lower than that of CHB) and formed a thin sediment of a few micrometers, as can be seen in Fig. 5. This behavior is similar to what we found for unlocked but labeled PMMA particles (see Fig. 3a in the main article). We therefore conclude that the use of labeled PMMA does not significantly influence the particle charge.

We also tried to measure the charge for these particles, but found that the charge was too low to be measured with the methods described in our article. We intend to address this in future work.

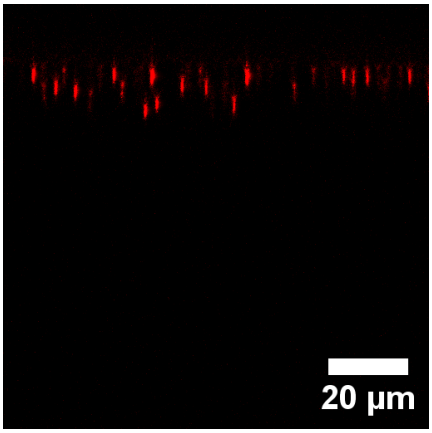

Figure 5: Confocal image showing a sediment of unlocked PMMA particles containing a small fluorescently labeled silica core in purified CHB.

References

[1] E. J. W. Verwey and J. Th. G. Overbeek, *Theory of the stability of lyophobic colloids.* Elsevier, Amsterdam, 1948.

[2] S. Alexander, P. M. Chaikin, P. Grant, G. J. Morales, P. Pincus, and D. Hone, "Charge renormalization, osmotic pressure, and bulk modulus of colloidal crystals: theory," *J. Chem. Phys.*, vol. 80, pp. 5776–5781, 1984.

[3] M. E. Leunissen, C. G. Christova, A.-P. Hynninen, C. P. Royall, A. I. Campbell, A. Imhof, M. Dijkstra, R. van Roij, and A. van Blaaderen, "Ionic colloidal crystals of oppositely charged particles," *Nature*, vol. 437, pp. 235–240, 2005.

[4] C. P. Royall, M. E. Leunissen, and A. van Blaaderen, "A new colloidal model system to study long-range interactions quantitatively in real space," *J. Phys.: Condens. Matter*, vol. 15, pp. S3581–S3596, 2003.

[5] R. J. Hunter, *Zeta potential in colloid science. Principles and applications.* Academic Press, London, 1981.

[6] R. M. Fuoss, "Ionic association. III. The equilibrium between ion pairs and free ions," *J. Am. Chem. Soc.*, vol. 80, pp. 5059–5061, 1958.

[7] Ph. C. van der Hoeven and J. Lyklema, "Electrostatic stabilization in non-aqueous media," *Adv. Colloid Interface Sci.*, vol. 42, pp. 205–277, 1992.

[8] G. S. Roberts, R. Sanchez, R. Kemp, T. Wood, and P. Bartlett, "Electrostatic charging of nonpolar colloids by reverse micelles," *Langmuir*, vol. 24, pp. 6530–6541, 2008.

[9] C. P. Royall, M. E. Leunissen, A.-P. Hynninen, M. Dijkstra, and A. van Blaaderen, "Re-entrant melting and freezing in a model system of charged colloids," *J. Chem. Phys.*, vol. 124, p. 244706, 2006.

[10] M. E. Leunissen, *Manipulating colloids with charges & electric fields.* PhD thesis, Utrecht University, The Netherlands, 2007. A digital version of this thesis is available at http://www.colloid.nl.

[11] R. M. Fuoss, "Dependence of the Walden product on dielectric constant," *Proc. Natl. Acad. Sci.*, vol. 45, pp. 807–813, 1959.

[12] G. J. Janz and S. S. Danyluk, "Conductances of hydrogen halides in anhydrous polar organic solvents," *Chem. Rev.*, vol. 60, pp. 209–234, 1960.

[13] G. Bosma, C. Pathmamanoharan, E. H. A. de Hoog, W. K. Kegel, A. van Blaaderen, and H. N. W. Lekkerkerker, "Preparation of monodisperse, fluorescent PMMA-latex colloids by dispersion polymerization," *J. Colloid Interface Sci.*, vol. 245, pp. 292–300, 2002.

[14] S. Siggia and J. Hanna, "Determination of organic isocyanates and isothiocyanates," *Anal. Chem.*, vol. 20, p. 1084, 1948.

[15] T. A. Fayed, M. H. Shaaban, M. N. El-Nahass, and F. M. Hassan, "Chalcones isothiocyanate anchored into mesoporous silicate: Synthesis, characterization and metal ions sensing response," *Microporous and Mesoporous Materials*, vol. 198, pp. 144–152, 2014.

[16] N. A. M. Verhaegh and A. van Blaaderen, "Dispersions of rhodamine-labeled silica spheres - Synthesis, characterization, and fluorescence confocal scanning laser microscopy," *Langmuir*, vol. 10, pp. 1427–1438, 1994.

[17] A. van Blaaderen and A. Vrij, "Synthesis and characterization of colloidal dispersions of fluorescent, monodisperse silica spheres," *Langmuir*, vol. 8, pp. 2921–2931, 1992.